

Polymer Stress Contribution in Turbulent Boundary Layer Drag Reduction

Y.X. Hou, V. S. R. Somandepalli and M. G. Mungal

Mechanical Engineering Department,
Stanford University, Stanford, CA 94305, USA
mungal@stanford.edu

ABSTRACT

In this work we investigate zero pressure gradient (ZPG) turbulent boundary layer (TBL) drag reduction (DR) by polymer injection using PIV. Flow fields ranging from low drag reduction to maximum drag reduction (MDR) have been investigated. A previously developed technique - the $(1-y)$ fit to the total shear stress profile - has been used to evaluate the skin friction, drag reduction and polymer stress. The polymer stress is found to be proportional to drag reduction in the drag depletion region but not necessarily so in the development and steady-state regions.

The stress balance in the boundary layer and the dynamical contribution of the various stresses to the total wall stress are evaluated following the approach of White *et al.* (2006). The results show that the polymer stresses can account for up to 25% of the skin friction at MDR conditions, with lesser contributions at lower drag reductions. This is in contrast to drag reduced channel flow data for homogeneous polymer distribution where the polymer stresses can be up to 60% of the skin friction at MDR.

INTRODUCTION

The addition of dilute polymer solutions to turbulent wall bounded flows can cause a significant reduction in the skin friction drag. This drag reducing effect of polymers, called the Toms effect, has been well known for more than 50 years. This reduction in skin friction, if applied to practical systems optimally, can lead to significant savings in fuel and travel time of ships and submarines.

The reduction of the skin friction due to polymer addition causes modification of the mean velocity profile (Virk 1975), changes in the turbulence structure and vorticity in the flow and leads to a redistribution of the stresses in the fluid. This interaction of the polymer solution with the near wall turbulence and its subsequent modification of the self sustaining mechanism of near wall turbulence (Jimenez & Pinelli, 1999) are profoundly important to the understanding of the mechanism of polymer DR. Past studies (e.g. Oldaker & Tiederman 1977, McComb & Rabie 1982, Warholic *et al.* 2001) to understand the physics of DR due to polymers have been mainly concentrated on cases with a homogeneous distribution of polymers in a pipe or channel flow, i.e., an ocean of polymer flowing through a pipe/channel. These flow fields are not representative of practical external flow applications of polymer DR with wall injection since these applications involve inhomogeneous polymer concentrations in developing turbulent boundary layers (TBL) where the polymer injection first leads to a development region of increasing DR, a steady-state region of DR and finally a depletion region of decreasing DR as

the polymer diffuses away from the wall. The present work examines the TBL case, following Wu & Tulin (1972), Vdovin, & Smol'yakov (1981), Tiederman, Luchik & Bogard (1985), Fontaine, Petrie & Brungart (1992), Petrie & Fontaine (1996) and Petrie *et al.* (2003), but focuses primarily on the role of the polymer stress in drag reduction.

One important quantity to be determined in the study of DR is the wall shear stress. The total shear stress in the Newtonian ZPG TBL is the sum of the viscous and Reynolds shear stresses. In the polymer DR TBL, the total shear stress is composed of three quantities: viscous stress, Reynolds shear stress, and polymer stress. Equation 1 is used to calculate the total shear stress in dilute polymer flow (Min *et al.* 2003).

$$\tau_{total} = \tau_p + \mu \partial u / \partial y + \rho(-\overline{u'v'}) \quad (1)$$

Both $\partial u / \partial y$ and $-\overline{u'v'}$ in Equation 1 can be measured or evaluated directly but not the polymer stress τ_p . In a polymer drag-reduced flow, there is a 'stress deficit' if the $[\mu \partial u / \partial y + \rho(-\overline{u'v'})]$ profile is compared to the total shear stress profile due to the missing (i.e. unmeasured) polymer stress (Koskie & Tiederman 1991, Warholic, Massah & Hanratty 1999). It is this additional polymer stress which makes it difficult to evaluate the wall shear stress. White *et al.* (2006), following the approach of Fukagata *et al.* (2002), analyzed the dynamical contributions to the skin-friction in polymer drag reduced flow and derived Equation 2.

$$C_f = \underbrace{\frac{4(1-\delta^*)}{Re_\delta}}_I + 2 \underbrace{\int_0^1 2(1-y)(-\overline{u'v'}) dy}_{II} \quad (2)$$

$$+ 2 \underbrace{\int_0^1 (1-y)^2 (-\frac{\partial \overline{\tau}}{\partial y}) dy}_{III} + 2 \underbrace{\int_0^1 2(1-y) \overline{\tau}_p dy}_{IV}$$

Here, Re_δ is the boundary layer thickness Reynolds number, δ^* is the displacement thickness normalized by δ (taken to be δ_{99} in this work), y is the wall normal coordinate normalized by δ , $-\overline{u'v'}$ is the Reynolds shear stress normalized by U^2 , $\overline{\tau}$ is the total shear stress (normalized by ρU^2) that equals the sum of the viscous, Reynolds and polymer stresses, and $\overline{\tau}_p$ is the additional polymer stress term (normalized by ρU^2) for a polymer solution ($\overline{\tau}_p = 0$ for Newtonian fluid). Equation 2 shows that the wall shear stress is determined by four terms: viscous term (I), Reynolds stress (II), total stress gradient (III) and polymer stress (IV). The sum of these four terms, determine the skin friction with, possibly, a non-unique combination of them for a given value of skin friction.

Inspired by this analysis, Hou, Somandepalli & Mungal (2006) developed a technique, based upon the $(1-y)$ weighting of Eqn. 2, to determine the wall shear stress and

used it to obtain the polymer stress profile. The same technique has been applied in this study. Furthermore, the profile of the polymer stress and its relation to the observed DR are important for understanding the interaction between the polymer and the turbulence. Intuitively, one might guess that the polymer stress is proportional to the DR, i.e., the larger the polymer stress, the higher the DR value. However, the polymer stress has not been studied extensively so the present study will concentrate on the polymer stress development.

Parallel to experimental studies, there are many studies of polymer DR flows via simulations, to name a few, Den Toonder *et al.* (1997), Dimitropoulos, Sureshkumar & Beris (1998), Dimitropoulos *et al.* (2001), Sibilla & Baron (2002), Dubief *et al.* (2004), Min *et al.* (2003), Terrapon *et al.* (2004), and Paschkewitz *et al.* (2005). Such numerical simulations have the ability to provide more details of the flow field than experimental studies. However, modeling of the polymer dynamics is typically required in these simulations and hence experimental results are needed for the purpose of comparison and validation of these models.

In a broader context, the present work attempts to systematically study DR in a TBL using PIV to obtain velocity and turbulence statistics data and provide information that was not obtained in previous studies. Various concentrations of polymer solutions are injected into a ZPG TBL and the DR is studied at various streamwise locations. The data provide a quantitative measure of the polymer effects on near wall turbulence. The data can also be used to validate models for simulating polymer DR and can help in formulating new models that better capture the physics of inhomogeneous polymer DR. A full description of all the results of this work can be found in Hou, Somandepalli & Mungal (2007).

EXPERIMENTAL DETAILS

The experiments were conducted in a constant head closed circuit water tunnel maintained at a ZPG condition, with a detailed description of the water tunnel facility given in White *et al.* (2004). The test section had a cross section of 0.36 m in span and 0.13 m in height with a length of 3.66 m. The walls of the tunnel were constructed from acrylic to provide full optical access to the top wall which served as the test surface. The flow inlet velocity was maintained constant at 0.5 m/s while the temperature was maintained at a constant value of 18 ± 0.2 °C. The leading edge of the test wall was a half ellipse with major to minor axis ratio of 16. A 0.6 mm diameter rod glued 25.4 mm downstream of the leading edge was used to trip the boundary layer and make it turbulent.

Table 1 gives a comprehensive listing of the boundary layer parameters at each of the measurement stations. There are six measurement positions on the flat plate designated *x02*, *x06*, *x1*, *x2*, *x3* and *x4*. The injection slot was located between position *x02* and *x06* and was 483 mm downstream of the plate's leading edge. For a purely Newtonian boundary layer with a freestream velocity of 0.5 m/s, the boundary layer thickness varied from 13 mm at position *x02* to 42 mm at position *x4*.

PIV was used to measure velocity and velocity statistics in these experiments. The PIV system used a Peltier cooled 12 bit CCD camera with a resolution of 1280×1024 pixels,

a dual head - pulsed Nd:YAG laser operating at 532nm, and appropriate sheet forming optics. The flow was naturally seeded with residual dust particles in the water of size less than 10 microns. One thousand image pairs were acquired at each streamwise location to ensure good convergence of higher order turbulence statistics. The PIV processing used a multi-pass iterative scheme starting with a cross-correlation window boxsize of 64×64 pixels and a final pass at 32×32 pixels with 50% overlap between adjacent correlation regions. The spatial resolution of the camera was $13.6 \mu\text{m}$ per pixel with an effective field of view of $17.4 \text{ mm} \times 13.9 \text{ mm}$. The smallest scale resolved was $435 \mu\text{m}$.

Table 1 Newtonian TBL parameters. x = distance from leading edge; δ = boundary layer thickness at $u/U = 99\%$; θ = momentum thickness, and Re_θ = Reynolds number based on momentum thickness = $U\theta/\nu$.

Typical TBL parameters for $U = 0.5 \text{ m/s}$					
Position	x (mm)	x^+ (based on local u_τ)	δ (mm)	θ (mm)	Re_θ
<i>x02</i>	343	7690	13	1.6	730
Inj. slot	483	10640	15	1.8	840
<i>x06</i>	597	12900	17	2.1	970
<i>x1</i>	737	15320	20	2.5	1150
<i>x2</i>	1168	23320	27	3.5	1620
<i>x3</i>	1651	31310	35	4.5	2060
<i>x4</i>	2108	39400	41	5.2	2380

The polymer used was poly-ethylene oxide (PEO) WSR-301 from Dow Chemical Co. The mean molecular weight, based on the manufacturer's specification sheet, was ~ 4 million. The polymer solution was prepared by directly mixing the polymer powder with water which was filtered by a carbon filter to remove all contaminants and residual chlorine. After all polymer powder had been added to the solution, it was gently stirred for several hours periodically. The solutions were then allowed to stand for at least 20 hours to homogenize and allow degassing.

Polymer concentrations of 100, 250, 500, 1000 and 2000 wppm were investigated. The polymer solution was injected into the boundary layer through an injection slot by pressurizing its holding container slightly above the tunnel pressure ($\sim 41 \text{ kPa}$) with compressed air. The single injection slot was inclined at 30° to the flat plate and had dimensions of 0.45 mm width, 10 mm flow entrance length and 310 mm in span.

The injection rate of polymer is denoted by the ratio Q_i/Q_s , where Q_i is the flow rate of the injected fluid; Q_s ($= 67.3\nu$) is the volume flow rate of water in the viscous sublayer (defined by the sublayer edge at $y^+ = 11.6$) of the boundary layer and is independent of velocity. In order to minimize the disturbance of the injected flow on the boundary layer, Q_i should be smaller or on the same order as Q_s (Wu & Tulin 1972, Walker, Tiederman & Luchik 1986, Fontaine *et al.* 1992). The typical injection rate in the current experiment was about 0.77 so that the injection disturbance was small. The injector width in plus units is 11 and is thus within the sublayer. The injection velocity is high at 23% of the freestream velocity. However, as

discussed below, the overall disturbance to the flow due to injection is quite small and can be neglected.

RESULTS

Water Injection Results

To verify the accuracy of the measurement technique, the mean velocity profiles and Reynolds shear stress profiles with and without water injection were compared. The injection disturbance effect is found to be so small that there is essentially no difference in the mean velocity profiles in water injected and non-injected flows. There is some small initial difference in the Reynolds shear stress profiles, at position $x06$, but the difference disappears further downstream at positions $x2$ and $x4$. These results prove that the change of the boundary layer flow due to water injection is negligible and any changes seen in polymer injected flows are due to the effect of the injected polymer and not the injection process itself.

To further validate the quality of the ZPG TBL facility and the PIV measurement technique, the current u_{rms} data and Reynolds shear stress data are compared with those in Fernholz & Finley (1996). The current u_{rms} agrees very well with that from other sources for $y^+ > 10$. The current PIV measurement could not resolve u_{rms} correctly for $y^+ < 10$ and this is expected since the PIV measurement was not optimized for sublayer measurement. Furthermore, it is clear that there is no difference in u_{rms} between water injected flow and the corresponding non-injected flow. Finally, excellent agreement is obtained between the current Reynolds shear stress profiles and those from several other sources (Hou *et al.* 2007).

Polymer Injection Results

There are several ways to define the DR value. In this study, it is defined by $DR = 100 \times (\tau_{water} - \tau_{polymer}) / \tau_{water}$ where $\tau_{polymer}$ and τ_{water} are the skin friction (wall shear stress) of polymer flow and the corresponding Newtonian flow respectively.

Computing Skin Friction. A very important parameter to be measured in the current study is the skin friction for both Newtonian flow and polymer (*injected*) flow. There are many ways to obtain the skin friction for Newtonian flow, i.e., shear stress sensors or evaluation from the mean velocity profile by using the Clauser chart. The second method, the Clauser chart, is used in the current study for Newtonian flow. The skin friction of polymer flow, however, is problematic since evaluation from the mean velocity profile by the Clauser chart does not work. Hou *et al.* (2006) solved this problem by using a $(I-y)$ fit to the total shear stress profile to obtain the wall shear stress. The same fit is used here with the PIV data to estimate the skin friction and DR. Sometimes, however, the flow close to the injection slot is in the process of adjusting to the effect of injected polymer and, hence, is not in equilibrium and the $(I-y)$ fit fails to work in this region of flow adjustment. The value of DR in such a situation is estimated from the mean velocity profile slope (Hou *et al.* 2007). The slope of the mean velocity profile in DR flow, when plotted in semi-log format, increases with the value of DR (e.g. see Figures 3 & 10 of Warholic *et al.* 1999). When the $(I-y)$ approach failed in the situations where the flow is not in equilibrium, the

measured mean velocity profile is compared with those where the DR values are known and the wall shear stress estimated. The uncertainty of the wall shear stress obtained from the mean velocity profile is relatively higher than that obtained from the $(I-y)$ fit. Nevertheless, the uncertainty of the estimated DR value is within 10%.

Polymer Stress Estimation. As stated in the introduction, in the polymer DR flows, there is a ‘stress deficit’ if the $[\mu \partial u / \partial y + \rho(-\overline{u'v'})]$ profile is compared to the total shear stress profile, with the missing part being the polymer stress. Figure 1 shows a typical $[\mu \partial u / \partial y + \rho(-\overline{u'v'})]$ profile we obtained in polymer DR flow along with the best fit obtained from the $(I-y)$ method applied to the inner portion of the boundary layer. The vertical intercept is the wall shear stress. It is clearly seen that there is a ‘stress deficit’ associated with the polymer stress, as indicated by the arrow, equal to the difference between the measured total stress and the fitted stress. A full justification of the validity of this approach is given in Hou *et al.* (2006) to which the reader is referred.

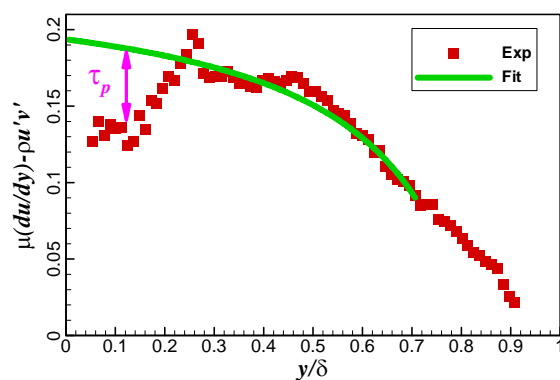


Figure 1. Shear stress in polymer injected flow, along with fit based upon $(I-y/\delta)$ method, fitted to $0 < y/\delta < 0.7$.

Polymer Stress Profiles

A typical example of the streamwise development of polymer stress profiles (derived from the approach shown in Fig. 1) for $C_i = 250$ wppm is shown in Fig. 2. The polymer stress shown is not normalized and has units of $\text{kg}/(\text{ms}^2)$, which is the same as the total shear stress in Fig. 1. The polymer stress is found to be significant for $y/\delta < 0.3$ and negligible in the outer part of the boundary layer. Interestingly, the polymer stress is found to be proportional to DR for the $C_i = 100$ wppm flow (not shown) but not for the $C_i = 250$ and 500 wppm flows. It may appear surprising that the magnitude of the polymer stress is not proportional to DR, i.e., high DR can correspond to low polymer stress. However the interaction between injected polymers and the turbulence in a developing boundary layer flow is complex and it produces an equally complex relationship between polymer stress and DR (Dimitropoulos *et al.* 2005), unlike the case of fully developed turbulent channel flows. By considering that the $C_i = 100$ wppm flow is entirely in the depletion region (i.e. the region of decaying DR), it is found that polymer stress is proportional to the DR value in this case.

Figure 3 shows the polymer stress at fixed streamwise positions for five different injection concentrations of 100, 250, 500, 1000, 2000 wppm. In general, for higher concentrations, it is found that polymer stress is not proportional to the DR value since the flows at that location are in different DR regions (development, steady-state, depletion) owing to the different injection concentrations.

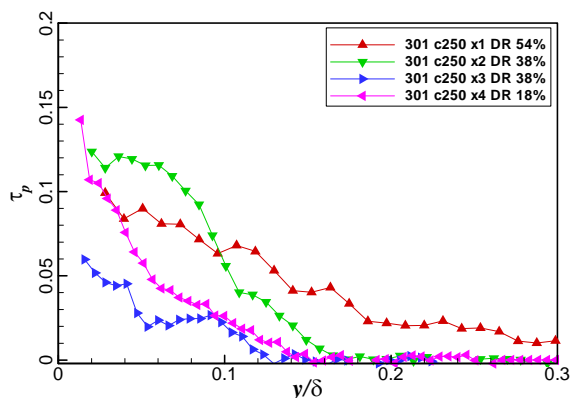


Figure 2. Streamwise development of the polymer stress for polymer concentration of 250 wppm and various downstream positions ($x1$, $x2$, $x3$, $x4$).

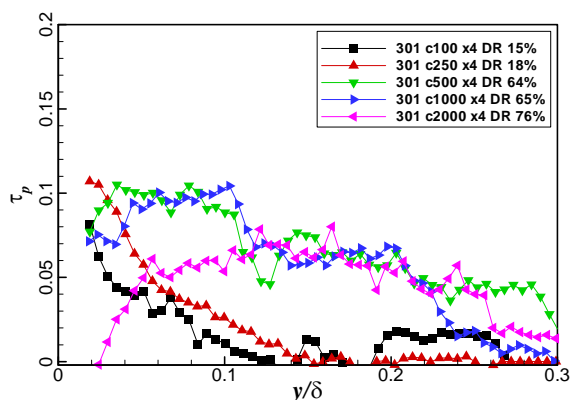


Figure 3. Polymer stress profiles at fixed streamwise location, $x4$, for different injection concentrations. DR values listed in caption.

The reason that polymer stress is not always proportional to DR can be rationalized by the following hypothetical mechanism of the polymer and turbulent activity interaction cycle: when the polymer is first injected into the TBL, it quickly becomes effective in reducing turbulent activity, leading to increased polymer stress and increasing DR in the development region; further downstream, in the steady state region (sometime the regions of high DR or MDR), the reduced turbulent intensity allows the polymer to be less stretched and still maintain high DR so that the polymer stress is not necessarily high. The relatively low polymer stress at high DR is also due to the fact that the skin friction (hence the total shear stress) is already reduced so that the magnitude of the polymer stress must be small. However the polymer stress can have very high contribution to the total shear stress, as will be shown in the stress balance section below. Even further downstream, in the depletion region, as the

turbulent activity regains strength, the DR begins to decrease while the remaining polymer near the wall becomes active and thus generates polymer stress. In this hypothetical cycle, the polymer stress and the drag reduction of the flow are not always synchronized since the turbulent state of the flow and polymer, and their integrated history, are important; there is potentially a phase lag associated with the polymer activity as it responds to the turbulence and this phase difference allows the possibility of high DR with low polymer stress. Hence there is not a one-to-one relationship between polymer stress and DR, except in the depletion region.

Dynamical Stress Balance in the TBL

With the total shear stress profiles and the polymer stress profiles obtained by using the (I - y) fitting, the dynamical contributions to the skin-friction in ZPG TBL flows (Equation 2) are evaluated by integrating each term directly with results shown in Table 2 for Newtonian flow and Tables 3-6 for polymer flows which have diluted sufficiently for the analysis to hold. The tables list the percentage contributions of each term to the skin friction, and the error in the predicted skin friction obtained from summing the four terms when compared to the measured value. The role of the polymer stress in the overall DR can thus be ascertained.

The Newtonian flow in Table 2 shows that the contributions of the viscous term (term I), Reynolds stress (term II) and total stress gradient (term III) to the skin friction are 5~9%, 65~70% and 20~23% respectively. The polymer flow at position $x1$ (DR = 45%) in Table 3 shows that the contribution of term I increases significantly to 16.6%. However, the absolute values (not shown) of term I are the same for both polymer flow and the corresponding Newtonian flow. The percentage increase of its contribution is only a result of the reduced skin friction. The contributions of term II and III are both reduced in polymer flow and the reductions are different at different conditions.

The general trend shown in Tables 3-6 is as follows: at upstream locations, term II is only slightly reduced while term III is significantly reduced; further downstream, the reduction of term II becomes more significant while the reduction of term III becomes less significant. This trend is best seen in the near MDR flow in Table 6 from position $x3$ (DR = 71%) to $x4$ (DR = 65%) - term II is reduced from 49.6% to 42.1%; while term III increases from 6.7% to 23.3%. For all the cases shown in Tables 3-6, the highest contribution of polymer stress (term IV) to the skin friction is about 25%, which shows that polymer stress can be an important contributor to the skin friction. The contribution of polymer stress is roughly proportional to the DR values for the cases shown in Tables 3-4, i.e., higher contribution of term IV in higher DR flow. This appears due to the fact that the flow in these two cases is in the DR depletion region. The contribution of polymer stress is not proportional to DR when the flow goes through different DR regions as shown in Table 5, where the DR increases from 50% ($x1$) to 69% ($x2$) (development region), then reduces slightly and finally remains constant from positions $x3$ to $x4$ (steady-state region).

The trend of the polymer stress contribution to the skin friction shown in Table 5 is consistent with the above

proposed polymer and turbulent activity interaction cycle. The contribution of term *IV* is higher at *x1* (DR = 50%) than that at *x2* (DR = 69%) because the flow is in the development region. In this region, the polymer is more active due to the strong turbulent activity in the incoming flow so that polymer stress has a bigger contribution. While at position *x2* (DR = 69%), the turbulent activity have been significantly reduced and the polymer is less active so that it has relatively smaller contribution. Further downstream, the DR decreases slightly which indicates that the turbulent activity becomes relatively stronger. As a result the polymers become more active again and hence polymer stress (term *IV*) has a bigger contribution.

Table 2 Dynamical contributions to the skin-friction in Newtonian ZPG TBL.

Newtonian Flow					
Posn	I%	II%	III%	IV%	Err%
<i>x1</i>	8.8	65.4	23.7	0	-2.1
<i>x2</i>	6.9	67.5	23.6	0	-2.0
<i>x3</i>	5.8	72.3	19.4	0	-2.5
<i>x4</i>	5.1	67.6	24.1	0	-3.2

Table 3 Dynamical contributions to the skin-friction in polymer flow with injection concentration of 100 wppm.

PEO WSR-301; Conc. = 100 wppm; Qi/Qs = 0.78						
Posn	DR	I%	II%	III%	IV%	Err%
<i>x1</i>	45	16.6	62.6	8.5	16.7	4.5
<i>x2</i>	34	10.7	60.7	22.1	9.3	2.8
<i>x3</i>	10	6.5	64.9	24.1	5.1	0.6
<i>x4</i>	15	6.6	68.4	21.1	5.8	1.9

Table 4 Dynamical contributions to the skin-friction in polymer flow with injection concentration of 250 wppm.

PEO WSR-301; Conc. = 250 wppm; Qi/Qs = 0.82						
Posn	DR	I%	II%	III%	IV%	Err%
<i>x1</i>	54	19.0	68.7	0.6	14.9	3.2
<i>x2</i>	38	11.1	60.0	20.0	11.2	2.2
<i>x3</i>	38	9.4	71.0	15.6	5.5	1.5
<i>x4</i>	18	6.2	61.6	28.2	5.9	1.9

Table 5 Dynamical contributions to the skin-friction in polymer flow with injection concentration of 500 wppm.

PEO WSR-301; Conc. = 500 wppm; Qi/Qs = 0.79						
Posn	DR	I%	II%	III%	IV%	Err%
<i>x1</i>	50	17.1	64.5	1.8	19.3	2.8
<i>x2</i>	69	21.5	52.7	7.4	17.6	-0.8
<i>x3</i>	61	14.6	41.6	16.5	27.0	-0.3
<i>x4</i>	64	14.0	45.4	16.5	24.5	0.3

Table 6 Dynamical contributions to the skin-friction in polymer flow with injection concentration of 1000 wppm.

PEO WSR-301; Conc. = 1000 wppm; Qi/Qs = 0.77						
Posn	DR	I%	II%	III%	IV%	Err%
<i>x3</i>	71	20.4	49.6	6.7	25.1	1.8
<i>x4</i>	65	14.7	42.1	23.3	20.5	0.6

Dynamical Stress Balance in Channel Flow

We compare the polymer stress in the TBL with inhomogeneous injection to those found in channel flows

with homogeneous polymer distribution. Such data have been provided by Warholic *et al.* (1999). To perform the analysis we note that the corresponding equation for the dynamical contributions in the channel flow is given by White *et al.* (2006) as

$$C_f = \underbrace{\frac{6}{Re_h}}_I + 6 \underbrace{\int_0^1 (1-y)(-\overline{u'v'})dy}_{II} + 6 \underbrace{\int_0^1 (1-y)\overline{\tau_p}dy}_{III} \quad (3)$$

where Re_h is the Reynolds number based on mean velocity, U_m , and channel half-height, h , y is the wall normal coordinate normalized by h , the Reynolds stress is normalized by U_m^2 and the polymer stress is normalized by ρU_m^2 . Using the data from Figs. 13 and 14 of Warholic *et al.* (1999) produces the results shown in Table 7. The agreement between DR and the prediction given by the sum of the three terms is quite satisfactory for water and most DR cases, with errors less than 4%. The exception is the DR = 64% case. Here the error comes from Term II since the measured Reynolds stress is very small leading to large digitization errors.

Table 7 Dynamical contributions to the skin-friction for homogeneous channel flow data of Warholic *et al.* (1999).

	I%	II%	III%	Err%
Water	8.8	91.2	0	N/A
DR=38%	15.0	60.4	23.2	-1.3
DR=55%	20.0	19.4	61.3	0.7
DR=64%	23.3	1.1	63.2	-12.4
DR=69%	28.4	9.9	57.9	-3.7

An important comparison of the homogeneous channel at MDR to the inhomogeneous TBL at MDR is that the former shows a polymer stress contribution of ~60% while the latter shows ~25%. This appears to be a fundamental difference associated with inhomogeneous and homogeneous distribution of polymer at MDR. In the inhomogeneous case the Reynolds stress is decreased significantly close to the wall, but less so further from the wall at MDR (Petrie & Fontaine 1996, Hou *et al.* 2007). The (I - y) weighting of Equations (1) and (2) suggests that contributions to the skin friction from the Reynolds stress away from the wall play a lesser role in the overall DR. In the homogeneous channel case, while the Reynolds stresses are reduced across the entire channel width, the (I - y) weighting still shows that it is primarily the reductions close to the wall that produce the dominant DR effect.

CONCLUSIONS

The data presented here provide a quantitative measure of the polymer effects on near wall turbulence with emphasis upon the polymer stress contributions in the TBL – an area which has received limited attention in the past. The data can also be used to validate models for simulating polymer DR and can help in formulating new models that better capture the physics of inhomogeneous polymer DR. The polymer stress is found to be proportional to drag reduction in the depletion region but not necessarily so in the development and steady-state DR regions. The results show that the polymer stresses can account for up to 25% of

the total skin friction at MDR conditions, with lesser contributions at lower drag reductions. This is in contrast to drag reduced channel flow data for homogeneous polymer distribution where the polymer stresses are responsible for up to 60% of the total skin friction at MDR.

ACKNOWLEDGEMENT

This work is sponsored by Defense Advanced Research Projects Agency (DARPA), Advanced Technology Office, Friction Drag Reduction Program, DARPA Order No.: K042/31, K042/13, N115/00, issued by DARPA/CMO, Contract No. MDA972-01-C-0041. The content does not necessarily reflect the position or the policy of the U.S. Government, and no official endorsement should be inferred. The authors thank Drs. Chris White and Yves Dubief for helpful discussions of DR in TBL.

REFERENCES

- Den Toonder, J., Hulsen, M., Kuiken, G. & Nieuwstadt, F. 1997 Drag reduction by polymer additives in a turbulent pipe flow: numerical and laboratory experiments. *J. Fluid Mech.* 337, 193–231.
- Dimitropoulos, C., Sureshkumar, R. & Beris, A. 1998 Direct numerical simulation of viscoelastic turbulent channel flow exhibiting drag reduction: effect of variation of rheological parameters. *J. Non-Newtonian Fluid Mech.* 79, 433–468.
- Dimitropoulos, C., Sureshkumar, R., Beris, A. & Handler, R. 2001 Budgets of Reynolds stress, kinetic energy and streamwise enstrophy in viscoelastic turbulent channel flow. *Phys. Fluids* 13, 1016–1027.
- Dimitropoulos C. D., Dubief Y., Shaqfeh E. S. G., Moin P. & Lele S. K. 2005 Direct numerical simulation of polymer-induced drag reduction in turbulent boundary layer flow. *Phys. Fluids* 17:011705.
- Dubief, Y., White, C., Terrapon, V. E., Shaqfeh, E., Moin, P. & Lele, S. 2004 On the coherent drag-reducing and turbulence-enhancing behaviour of polymers in wall flows. *J. Fluid Mech.* 514, 271–280.
- Fernholz H. H. & Finley P. J. 1996 The incompressible zero-pressure-gradient turbulent boundary layer: an assessment of the data. *Prog. Aerospace Sci.* 32:245-311.
- Fontaine, A. A., Petrie, H. L. & Brungart, T. A. 1992 Velocity profile statistics in a turbulent boundary layer with slot-injected polymer. *J. Fluid Mech.* 238:435 - 466.
- Fukagata, K., Iwamoto, K. & Kasagi, N. 2002 Contribution of Reynolds stress distribution to the skin friction in wall-bounded flows. *Phys. Fluids*, 14(11): L73 - 76.
- Hou, Y. X., Somandepalli, V. S. R. & Mungal, M. G. 2006 A technique to determine total shear stress and polymer stress profiles in drag reduced boundary layer flows. *Experiments in Fluids*, 40, 589-600.
- Hou, Y. X., Somandepalli, V. S. R. & Mungal, M. G. 2007 Streamwise Development of Turbulent Boundary Layer Drag Reduction with Polymer Injection. Submitted to *J. Fluid Mech.*
- Jimenez, J. & Pinelli, A. 1999 The autonomous cycle of near wall turbulence. *J. Fluid Mech.* 398:335-339.
- Koskie, J. E. & Tiederman, W. G. 1991 Polymer drag reduction of a zero-pressure-gradient boundary layer. *Phys. Fluids* A3:2471–2473.
- McComb, W. D. & Rabie, L. H. 1982 Local drag reduction due to injection of polymer solution into turbulent flow in a pipe. Part I: dependence on local polymer concentration; and Part II: laser Doppler measurements of turbulence structure. *AIChE Journal.* 28:547–565.
- Min, T., Yoo, J. Y., Choi, H. & Joseph, D. D. 2003 Drag reduction by polymer additives in a turbulent channel flow. *J. Fluid Mech.* 486:213–238.
- Oldaker, D. K. & Tiederman, W. G. 1977 Structure of the turbulent boundary layer in drag reducing pipe flow. *Phys. Fluids* 20:133-144.
- Paschkewitz, J. S., Dimitropoulos, C. D., Hou, Y. X., Somandepalli, V. S. R., Mungal, M. G., Shaqfeh, E. S. G. & Moin, P. 2005 An experimental and numerical investigation of drag reduction in a turbulent boundary layer using a rigid rodlike polymer. *Phys. Fluids* 17, 085101.
- Petrie, H. L. & Fontaine, A. A. 1996 Comparison of turbulent boundary layer modifications with slot-injected and homogeneous drag-reducing polymer solutions, Proceedings of the Fluids Engineering Division Conference. *ASME* 2:205-210.
- Petrie, H. L., Deutsch, S., Brungart, T. A. & Fontaine, A. A. 2003 Polymer drag reduction with surface roughness in flat-plate turbulent boundary layer flow. *Exp. Fluids* 35:8–23.
- Sibilla, S. & Baron, A. 2002 Polymer stress statistics in the near-wall turbulent flow of a drag reducing solution. *Phys. Fluids* 14, 1123–1136.
- Terrapon, V., Dubief, Y., Moin, P., Shaqfeh, E. & Lele, S. 2004 Simulated polymer stretch in a turbulent flow using Brownian dynamics. *J. Fluid Mech.* 504, 61–71.
- Tiederman, W. G., Luchik, T. S. & Bogard, D. G. 1985 Wall layer structure and drag reduction. *J. Fluid Mech.* 156:419-437.
- Vdovin, A. V. & Smol'yakov, A. V. 1981 Turbulent diffusion of polymers in a boundary layer. *Zh. Prikl. Mekh. Tekh. Fiz.* 4:98-104 (transl. in UDC532.526(1982) 526-531, Plenum).
- Virk, P. S. 1975 Drag reduction fundamentals. *AIChE J.* 22:625-656.
- Walker, D. T., Tiederman W. G. & Luchik T. S. 1986 Optimization of the injection process for drag reduction additives. *Exp. Fluids* 4, 114-120.
- Warholic, M. D., Massah, H. & Hanratty, T. J. 1999 Influence of drag-reducing polymers on turbulence: effects of Reynolds number, concentration and mixing. *Exp. Fluids* 27:461–472.
- Warholic, M. D., Heist, D. K., Katcher, M. & Hanratty, T. J. 2001 A study with particle image velocimetry of the influence of drag reducing polymers on the structure of turbulence. *Exp. Fluids* 31:474-483.
- White, C. M., Somandepalli, V. S. R. & Mungal, M. G. 2004 The turbulence structure of drag-reduced boundary layer flow. *Exp. Fluids* 36:62-69.
- White, C. M., Somandepalli, V. S. R., Dubief, Y. & Mungal, M. G. 2006 Dynamical contributions to the skin friction in polymer drag reduced wall-bounded turbulence. Submitted to *Phys. Fluids*.
- Wu, J. & Tulin, M. P. 1972 Drag reduction by ejecting additive solutions into a pure water boundary layer. *Trans. ASME D: J. Basic Engng* 94, 749-755.